2

Multi-months cycles observed in climatic data

Samuel Nicolay, Georges Mabille, Xavier Fettweis and M. Erpicum
University of Liège
Belgium

1. Introduction

Climatic variations happen at all time scales and since the origins of these variations are usually of very complex nature, climatic signals are indeed chaotic data. The identification of the cycles induced by the natural climatic variability is therefore a knotty problem, yet the knowing of these cycles is crucial to better understand and explain the climate (with interests for weather forecasting and climate change projections). Due to the non-stationary nature of the climatic time series, the simplest Fourier-based methods are inefficient for such applications (see e.g. Titchmarsh (1948)). This maybe explains why so few systematic spectral studies have been performed on the numerous datasets allowing to describe some aspects of the climate variability (e.g. climatic indices, temperature data). However, some recent studies (e.g. Matyasovszky (2009); Paluš & Novotná (2006)) show the existence of multi-year cycles in some specific climatic data. This shows that the emergence of new tools issued from signal analysis allows to extract sharper information from time series.
Here, we use a wavelet-based methodology to detect cycles in air-surface temperatures obtained from worldwide weather stations, NCEP/NCAR reanalysis data, climatic indices and some paleoclimatic data. This technique reveals the existence of universal rhythms associated with the periods of 30 and 43 months. However, these cycles do not affect the temperature of the globe uniformly. The regions under the influence of the AO/NAO indices are influenced by a 30 months period cycle, while the areas related to the ENSO index are affected by a 43 months period cycle; as expected, the corresponding indices display the same cycle. We next show that the observed periods are statistically relevant. Finally, we consider some mechanisms that could induce such cycles. This chapter is based on the results obtained in Mabille & Nicolay (2009); Nicolay et al. (2009; 2010).

2. Data

2.1 GISS temperature data

The Goddard Institute for Space Studies (GISS) provides several types of data.
The GISS temperature data (Hansen et al. (1999)) are made of temperatures measured in weather stations coming from several sources: the National Climatic Data Center, the United States Historical Climatology Network and the Scientific Committee on Antarctic Research. These data are then reconstructed and "corrected" to give the GISS temperature data.
The temperatures from the Global Historical Climatology Network are also used to build temperature anomalies on a $2^\circ \times 2^\circ$ grid-box basis. These data are then gathered and "corrected" to obtain hemispherical temperature data (HN-T for the Northern Hemisphere and HS-T for the Southern Hemisphere) and global temperature data (GLB-T).

2.2 CRU global temperature data

The Climate Research Unit of the East Anglia University (CRU) provides several time series related to hemispherical and global temperature data (Jones et al (2001)). All these time series are obtained from a $5^\circ \times 5^\circ$ gridded dataset: CRUTEM3 gives the land air temperature anomalies (CRUTEM3v is a variance-adjusted version of CRUTEM3), HadSST2 gives the sea-surface temperature (SST) anomalies and HadCRUT3 combines land and marine temperature anomalies (a variance-adjusted version of these signals is available as well). For each time series, a Northern Hemispheric mean, a Southern Hemispheric mean and a global mean exist.

2.3 NCEP/NCAR reanalysis

The National Centers for Environmental Prediction (NCEP) and the National Center for Atmospheric Research (NCAR) cooperate to collect climatic data: data obtained from weather stations, buoys, ships, aircrafts, rawinsondes and satellite sounders are used as an input for a model that leads to $2.5^\circ \times 2.5^\circ$ datasets (humidity, windspeed, temperature,...), with 28 vertical levels (Kalnay et al. (1996)). Only the near-surface air temperature data were selected in this study.

2.4 Indices

The Arctic oscillation (AO) is an index obtained from sea-level pressure variations poleward of 20N. Roughly speaking, the AO index is related to the strength of the Westerlies. There are two different, yet similar, definitions of the AO index : the AO CPC (Zhou et al. (2001)) and the AO JISAO.

The North Atlantic Oscillation (NAO) is constructed from pressure differences between the Azores and Iceland (NAO CRU, Hurrel (1995)) or from the 500mb height anomalies over the Northern Hemisphere (NAO CPC, Barnston & Livezey (1987)). This index also characterizes the strength of the Westerlies for the North Atlantic region (Western Europe and Eastern America).

The El Niño/Southern Oscillation (ENSO) is obtained from sea-surface temperature anomalies in the equatorial zone (global-SST ENSO) or is constructed using six different variables, namely the sea-level pressure, the east-west and north-south components of the surface winds, the sea-surface temperature, the surface air temperature and the total amount of cloudiness (Multivariate ENSO Index, MEI, Wolter & Timlin (1993; 1998)). This index is used to explain sea-surface temperature anomalies in the equatorial regions.

The Southern Oscillation Index (SOI, Schwing et al. (2002)) is computed using the difference between the monthly mean sea level pressure anomalies at Tahiti and Darwin.

The extratropical-based Northern Oscillation index (NOI) and the extratropical-based Southern Oscillation index (SOI*) are characterized from sea level pressure anomalies of the North Pacific (NOI) or the South Pacific (SOI*). They reflect the variability in equatorial and extratropical teleconnections (Schwing et al. (2002)).

The Pacific/North American (PNA, Barnston & Livezey (1987)) an North Pacific (NP, Trenberth & Hurrell (1994)) indices reflect the air mass flows over the north pacific. The PNA index is defined over the whole Northern Hemisphere, while the NP index only takes into account the region 30N–65N, 160E–140W.

The Pacific Decadal Oscillation (PDO, Mantua et al (1997)) is derived from the leading principal component of the monthly sea-surface temperature anomalies in the North Pacific Ocean, poleward 20N.

3. Method

3.1 The continuous wavelet transform

The wavelet analysis has been developed (in its final version) by J. Morlet and A. Grossman (see Goupillaud et al. (1984); Kroland-Martinet et al. (1987)) in order to minimize the numerical artifacts observed when processing seismic signals with conventional tools, such as the Fourier transform. It provides a two-dimensional unfolding of a one-dimensional signal by decomposing it into scale (playing the role of the inverse of the frequency) and time coefficients. These coefficients are constructed through a function ψ, called the wavelet, by means of dilatations and translations. For more details about the wavelet transform, the reader is referred to Daubechies (1992); Keller (2004); Mallat (1999); Meyer (1989); Torresani (1995).
Let s be a (square integrable) signal; the continuous wavelet transform is the function W defined as

$$W[s](t,a) = \int s(x)\bar{\psi}(\frac{x-t}{a})\,\frac{dx}{a},$$

where $\bar{\psi}$ denotes the complex conjugate of ψ. The parameter $a > 0$ is the scale (i.e. the dilatation factor) and t the time translation variable. In order to be able to recover s from $W[s]$, the wavelet ψ must be integrable, square integrable and satisfy the admissibility condition

$$\int \frac{|\hat{\psi}(\omega)|^2}{|\omega|}\,d\omega < \infty,$$

where $\hat{\psi}$ denotes the Fourier transform of ψ. In particular, this implies that the mean of ψ is zero,

$$\int \psi(x)\,dx = 0.$$

This explains the denomination of wavelet, since a zero-mean function has to oscillate.
The wavelet transform can be interpreted as a mathematical microscope, for which position and magnification correspond to t and $1/a$ respectively, the performance of the optic being determined by the choice of the lens ψ (see Freysz et al. (1990)).
The continuous wavelet transform has been successfully applied to numerous practical and theoretical problems (see e.g. Arneodo et al. (2002); Keller (2004); Mallat (1999); Nicolay (2006); Ruskai et al. (1992)).

3.2 Wavelets for frequency-based studies

One of the possible applications of the continuous wavelet transform is the investigation of the frequency domain of a function. For more details about wavelet-based tools for frequency analysis, the reader is referred to Mallat (1999); Nicolay (2006); Nicolay et al. (2009); Torresani (1995).
Wavelets for frequency-based studies have to belong to the second complex Hardy space. Such a wavelet is given by the Morlet wavelet ψ_M whose Fourier transform is given by

$$\hat{\psi}_M(\omega) = \exp(-\frac{(\omega-\Omega)^2}{2}) - \exp(-\frac{\omega}{2})\exp(-\frac{\Omega}{2}),$$

where Ω is called the central frequency; one generally chooses $\Omega = \pi\sqrt{2/\log 2}$. For such a wavelet, one directly gets

$$W[\cos(\omega_0 x)](t,a) = \frac{1}{2}\exp(i\omega_0 t)\hat{\psi}_M(a\omega_0).$$

Since the maximum of $\hat{\psi}_M(\cdot\omega_0)$ is reached for $a = \Omega/\omega_0$, if a_0 denotes this maximum, one has $\omega_0 = \Omega/a_0$. The continuous wavelet transform can thus be used in a way similar to the windowed Fourier transform, the role of the frequency being played by the inverse of the scale (times Ω).
There are two main differences between the wavelet transform and the windowed Fourier transform. First, the scale a defines an adaptative window: the numerical support of the function $psi(./a)$ is smaller for higher frequencies. Moreover, if the first m moments of the wavelet vanish, the associated wavelet transform is orthogonal to lower-degree polynomials, i.e. $W[s+P] = W[s]$, where P is a polynomial of degree lower than m. In particular, trends do not affect the wavelet transform.
In this study, we use a slightly modified version of the usual Morlet wavelet with exactly one vanishing moment,

$$\hat{\psi}(\omega) = \sin(\frac{\pi\omega}{2\Omega}) \exp(-\frac{\omega-\Omega)^2}{2}).$$

3.3 The scale spectrum

Most of the Fourier spectrum-based tools are rather inefficient when dealing with non-stationary signals (see e.g. Titchmarsh (1948)). The continuous wavelet spectrum provides a method that is relatively stable for signals whose properties do not evolve too quickly: the so-called scale spectrum. Let us recall that we are using a Morlet-like wavelet.
The scale spectrum of a signal s is

$$\Lambda(a) = E|W[s](t,a)|,$$

where E denotes the mean over time t. Let us remark that this spectrum is not defined in terms of density. Nevertheless, such a definition is not devoid of physical meaning (see e.g. Huang et al. (1998)). It can be shown that the scale spectrum is well adapted to detect cycles in a signal, even if it is perturbed with a coloured noise or if it involves "pseudo-frequencies" (see Nicolay et al. (2009)).
As an example, let us consider the function $f = f_1 + f_2 + \epsilon$, where $f_1(x) = 8\cos(2\pi x/12)$,

$$f_2(x) = (0.6 + \frac{\log(x+1)}{16}) \cos(\frac{2\pi}{30} x(1 + \frac{\log(x+1)}{100}))$$

and (ϵ) is an autoregressive model of the first order (see e.g. Janacek (2001)),

$$\epsilon_n = \alpha\epsilon_{n-1} + \sigma\eta_n,$$

where (η) is a centered Gaussian white noise with unit variance and $\alpha = 0.862$, $\sigma = 2.82$. The parameters α and σ have been chosen in order to simulate the background noise observed in the surface air temperature of the Bierset weather station (see Section 4). The function f (see Fig. 1) has three components: an annual cycle f_1, a background noise (ϵ) and a third component f_2 defined through a cosine function whose phase and amplitude evolve; f_2 is represented in Fig. 2. As we will see, such a component is detected in many climatic time series. As shown in Fig. 3, the scale spectrum of f displays two maxima, associated with the cycles of 12 months and 29.56 months respectively. The components f_1 and f_2 are thus detected, despite the presence of the noise (ϵ). Furthermore, the amplitudes associated with f_1 and f_2 are also recovered.

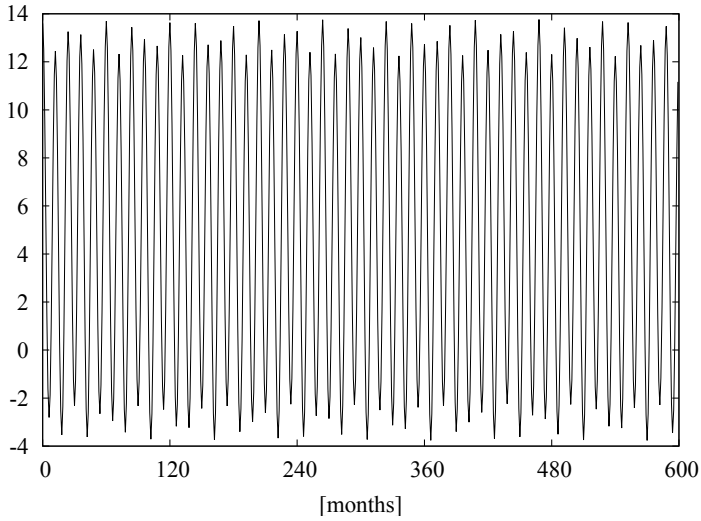

Fig. 1. The function f simulating an air surface temperature time series. The abscissa represent the months.

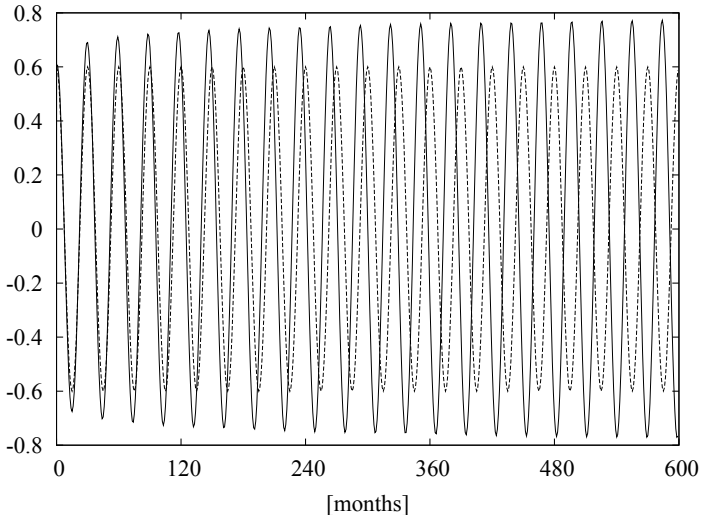

Fig. 2. The component f_2 (solid lines) of the function f, compared with the function $0.6\cos(2\pi x/30)$ (dashed lines). The abscissa represent the months.

Unlike the Fourier transform, which takes into account sine or cosine waves that persisted through the whole time span of the signal, the scale spectrum gives some likelihood for a wave to have appeared locally. This method can thus be used to study non-stationary signals.

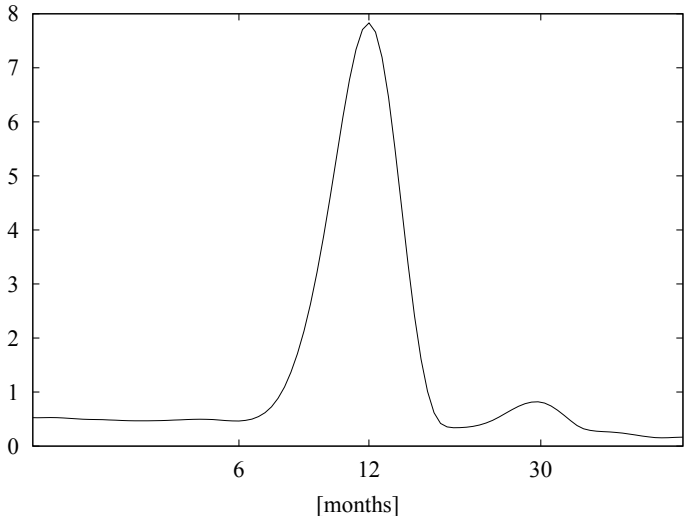

Fig. 3. The scale spectrum Λ of f. The abscissa (logarithmic scale) represent the months.

Let us remark that the scale spectra computed in this work do not take into account values that are subject to border effects.

4. Results

4.1 Scale spectra of global temperature records

The scale spectra of the global temperature data (CRUTEM3gl) display two extrema corresponding to the existence of two cycles $c_1 = 30 \pm 3$ months and $c_2 = 43 \pm 3$ months. The second cycle is also observed in the scale spectra of time series where the SST is taken into account (HadCRUT3, HadCRUT3v, HadSST2 and GLB-T). The existence of c_1 in these data is not so clear. The scale spectra of these series are shown in Fig. 4 and Fig. 5.

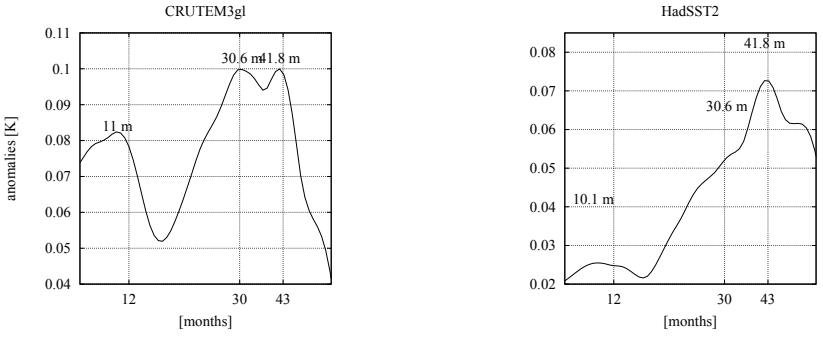

Fig. 4. The scale spectra of global temperature records. Crutem3 (left panel) and HadSST2 (right panel).

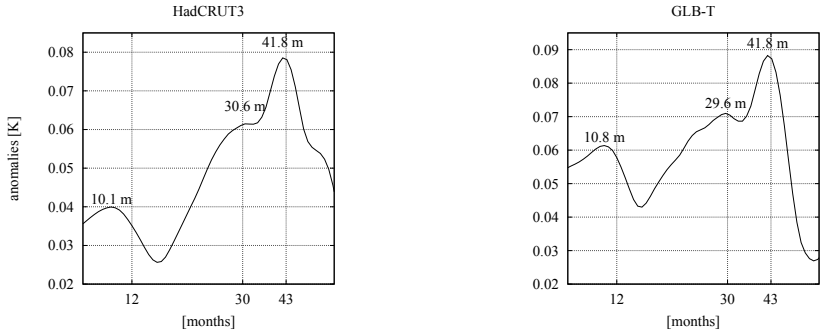

Fig. 5. The scale spectra of global temperature records: HadCRUT3 (left panel) and GLB-T (right panel).

When considering hemispheric data, c_1 and c_2 are still observed. The scale spectra of the global temperature time series in the Northern Hemisphere display a maximum corresponding to c_1. This cycle is more clearly observed in the data where the SST is not taken into account (i.e. with CRUTEM3nh), while c_2 is more distinctly seen in the other time series (NH-T, HadCrut3, HadSST2), as seen in Fig. 6 and Fig. 7. The spectra related to the Southern Hemisphere still display a maximum corresponding to c_2. For the CRU time series (HadCRUT3sh and HadSST2sh), the observed cycle that is the closest to c_1 is about 25 months, while the scale spectrum of the GISS data (SH-T) display a cycle c_1 as marked as the cycle c_2. The scale spectra of these series are shown in Fig. 8 and Fig. 9.

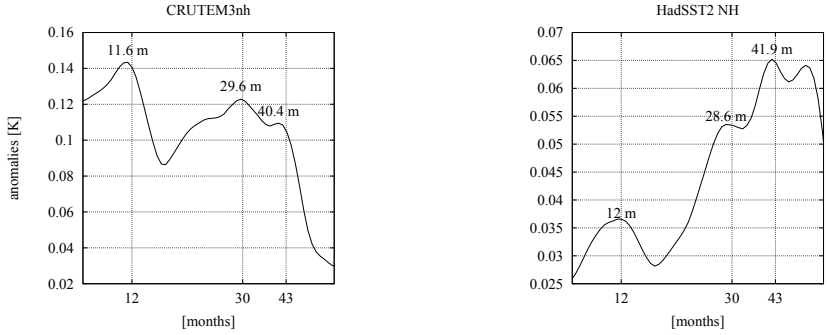

Fig. 6. The scale spectra of Northern Hemisphere temperature records: Crutem3 (left panel) and HadSST2 (right panel).

4.2 Scale spectra of local temperature records

In Nicolay et al. (2009), the scale spectra of a hundred near-surface air temperature time series have been computed using GISS Surface Temperature Analysis data (only the most complete data were chosen). The cycles detected in some weather stations are given by Fig. 10 and Table 1 (the location, the amplitude of the cycles found and the associated class of climate

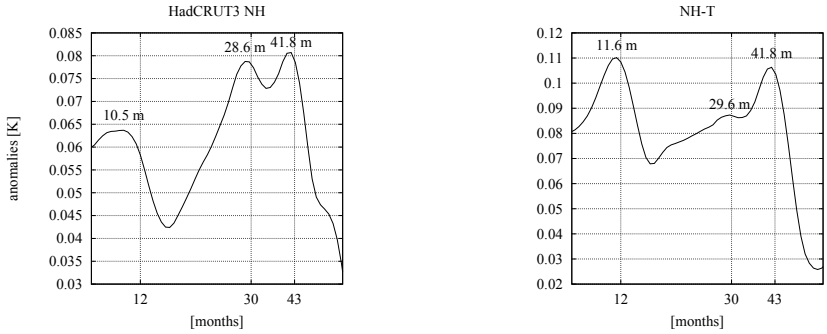

Fig. 7. The scale spectra of Northern Hemisphere temperature records: HadCRUT3 (left panel) and NH-T (right panel).

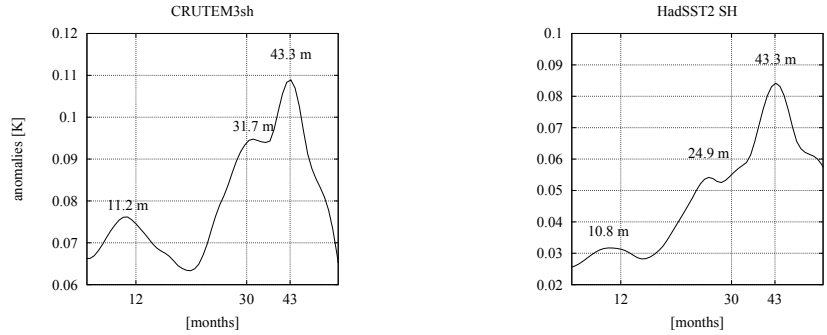

Fig. 8. The scale spectra of Southern Hemisphere temperature records: CRUTEM3 (left panel) and HadSST2 (right panel).

are also presented). These stations were selected in order to cover most of the typical climate areas (see for Rudloff (1981) more details). As expected, the scale spectrum leads to a correct estimation of the annual temperature amplitude (the difference between the mean temperature of the warmest and coldest months). The weather stations located in Europe and Siberia are clearly affected by the cycle c_1, while weather stations in areas such as California, Brazil, Caribbean Sea and Hawaii are influenced by c_2. The North American Weather stations time series analysis shows the presence of both c_1 and c_2. Roughly speaking, the temperature amplitudes induced by the cycles c_1 and c_2 represent about one tenth of the annual amplitude.

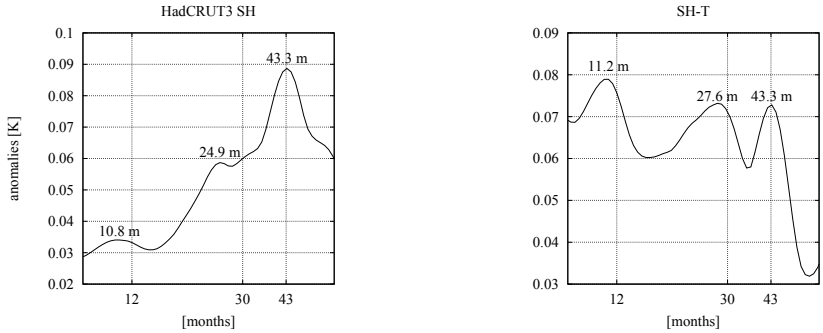

Fig. 9. The scale spectra of Southern Hemisphere temperature records: HadCRUT3 (left panel) and SH-T (right panel).

Weather stations	Lat.	Long.	Cycle (m)	Cycle amp.	An. amp.	Classif.
Uccle (Belgium)	50.8°N	4.3°E	30.4 ± 2.7	0.4 K	15 K	DO
Zaragoza (Spain)	41.6°N	0.9°W	28.4 ± 2.4	0.3 K	18 K	BS
The Pas (Canada)	54.0°N	101.1°W	28.5 ± 2.6	0.6 K	38 K	EC
			44.8 ± 2.4	0.8 K		
Fairbanks (Alaska)	64.8°N	147.9°W	28.5 ± 2.5	0.8 K	40 K	EC
			40.4 ± 2.5	0.8 K		
Verhojansk (Siberia)	67.5°N	133.4°E	31.7 ± 2.5	0.8 K	64 K	EC
Jakutsk (Siberia)	62.0°N	129.7°E	28.6 ± 2.4	0.8 K	60 K	EC
San Francisco (California)	37.6°N	122.4°W	41.8 ± 2.7	0.3 K	8 K	Cs
Lander (Wyoming)	42.8°N	108.7°W	41.8 ± 2.6	0.6 K	28 K	DC
Manaus (Brazil)	3.1°S	60.0°W	43.3 ± 2.4	0.3 K	3 K	Ar
Belo Horizonte (Brazil)	19.9°S	43.9°W	41.8 ± 2.4	0.5 K	4 K	Aw
Tahiti (French Polynesia)	17.6°S	149.6°W	41.8 ± 2.5	0.2 K	3 K	Ar
Lihue (Hawaii)	22.0°N	159.3°W	41.8 ± 2.5	0.3 K	4 K	Ar
Colombo (Sri Lanka)	6.9°N	79.9°E	44.5 ± 2.6	0.2 K	2 K	Ar
Minicoy (India)	8.3°N	73.2°E	41.8 ± 2.6	0.2 K	2 K	Aw

Table 1. Cycles found in some world weather stations (the errors are estimated as in Nicolay et al. (2009)). The stations were selected to represent the main climatic areas. For the class of climates, see Rudloff (1981).

To show, that c_1 and c_2 affect the whole planet, the scale spectrum of each grid point of the NCEP/NCAR reanalysis has been computed. As displayed in Fig. 11 and Fig. 12, 92% of the Earth area is associated to at least one of these cycles. Fig. 11 shows that c_1 is mainly seen in Alaska, Eastern Canada, Europe, Northern Asia and Turkey, while Fig. 12 reveals that c_2 is principally seen in Equatorial Pacific, Northern America and Peru. Roughly speaking, the cycle c_1 is observed in regions associated with the Arctic Oscillation, while c_2 is detected in regions associated to the Southern Oscillation.

4.3 Scale spectra of atmospheric indices

Advection causes the transfer of air masses to neighboring regions, carrying their properties such as air temperature. The climatic indices characterize these air mass movements.

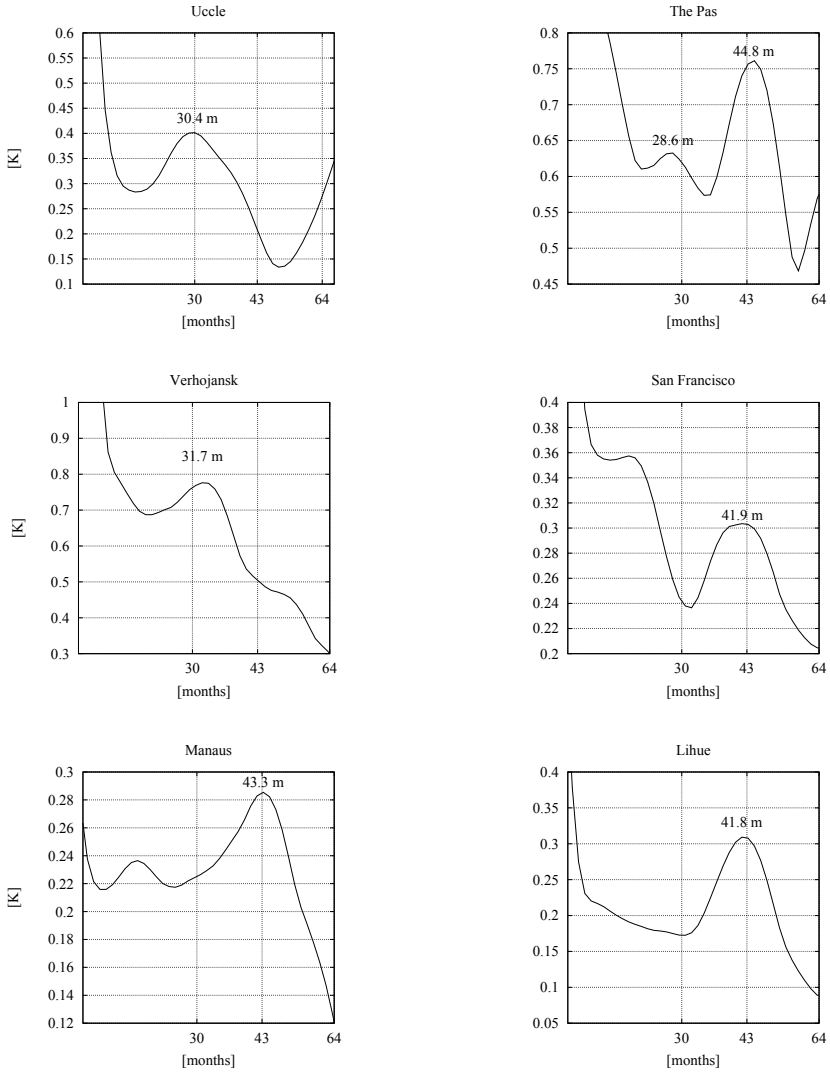

Fig. 10. Scale spectra of near-surface air temperature time series: Uccle (Belgium), The Pas (Canada), Verhojansk (Siberia), San Francisco (California), Manaus (Brazil), Lihue (Hawaii).

The cycles detected in the main climatic indices are reported in Table 2. Almost all these indices display a cycle corresponding to c_1, the notable exceptions being the NP, PNA and global-SST ENSO indices. The cycle c_2 is observed in the AO (CPC), NP, PDO, PNA and SOI* indices, as well as the indices related to the Southern Oscillation (such as the ENSO indices). The scale spectra of these indices are shown in Fig. 13, 14, 15 and 16.

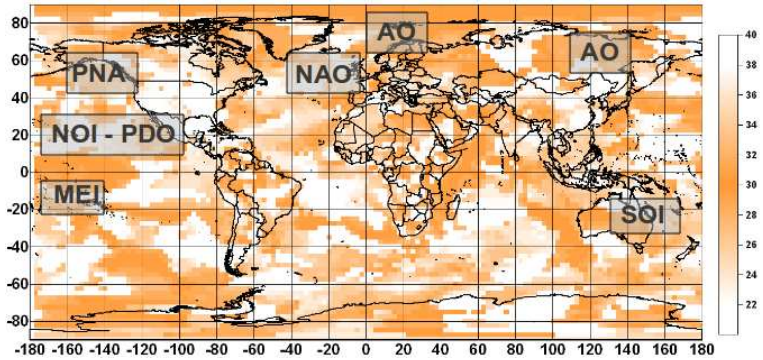

Fig. 11. NCEP/NCAR reanalysis data. The grid points where a cycle corresponding to c_1 has been detected are coloured.

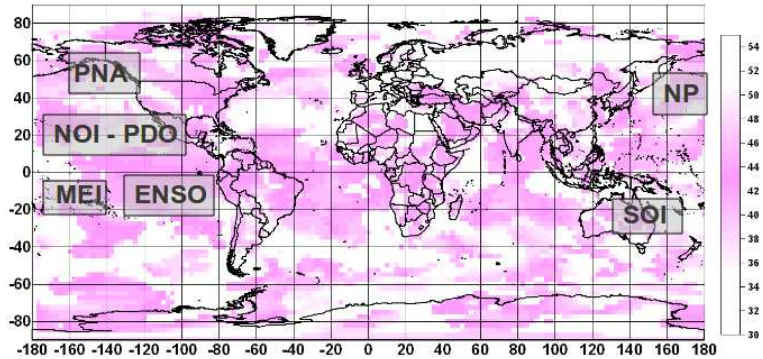

Fig. 12. NCEP/NCAR reanalysis data. The grid points where a cycle corresponding to c_2 has been detected are coloured.

Index	cycle c_1	cycle c_2
AO (CPC)	34 ± 2.6	43 ± 2.5
QBO	29 ± 2	
Global-SST ENSO		45 ± 2.1
MEI ENSO	30 ± 2.1	45 ± 2.1
NAO (CPC)	34 ± 2.1	
NAO (CRU)	34 ± 2.1	
NOI	32 ± 2.3	
NP		43 ± 2.4
PDO	26 ± 2.4	40 ± 2.3
PNA		45 ± 2.4
SOI	30 ± 2.2	
SOI*	30 ± 2.5	44 ± 2.6

Table 2. Cycles found in the main climatic indices (the errors are estimated as in Nicolay et al. (2009)).

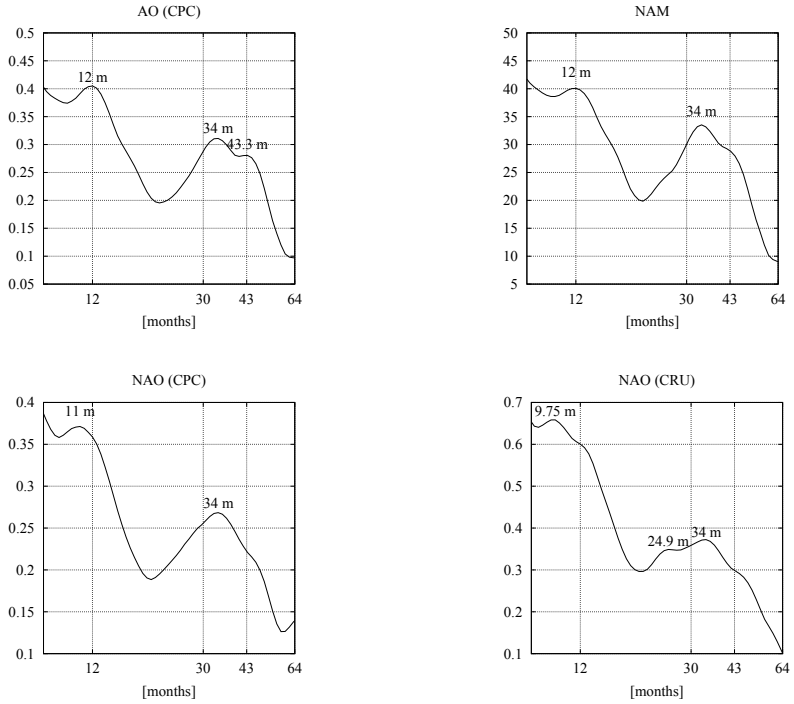

Fig. 13. Scale spectra of the climatic indices related to the Northern Atlantic Oscillation.

4.4 A statistical validation for the observed cycles

Although many evidences attest the validity of the method described above, a question naturally remains: Is there a high probability that the maxima observed in the scale spectra occurred by pure chance?

In Nicolay et al. (2010), to check if the cycles observed in the time series can be trusted, the scale spectra of the NCEP/NCAR reanalysis data have been compared with the spectra of signals made of an autoregressive model of the first order (AR(1) model, see e.g. Janacek (2001)), in which maxima could occur fortuitously. Such processes are observed in many climatic and geophysical data (see e.g. Allen & Robertson (1996); Percival & Walden (1993)) and are well suited for the study of climatic time series (see e.g. Mann & Lees (1996); Mann et al. (2007)).

An artificial signal (y_n) can be associated to the temperature time series (x_n) of a grid point of the NCEP/NCAR reanalysis data as follows:

- One first computes the climatological anomaly time series (δ_n) of (x_n), i.e. for each month, the mean temperature is calculated from the whole signal and the so-obtained monthly-sampled signal (m_n) is subtracted to (x_n), $\delta_n = x_n - m_n$.
- The anomaly time series (δ_n) is fitted with an AR(1) model (ϵ_n),

$$\epsilon_n = \alpha\epsilon_{n-1} + \sigma\eta_n,$$

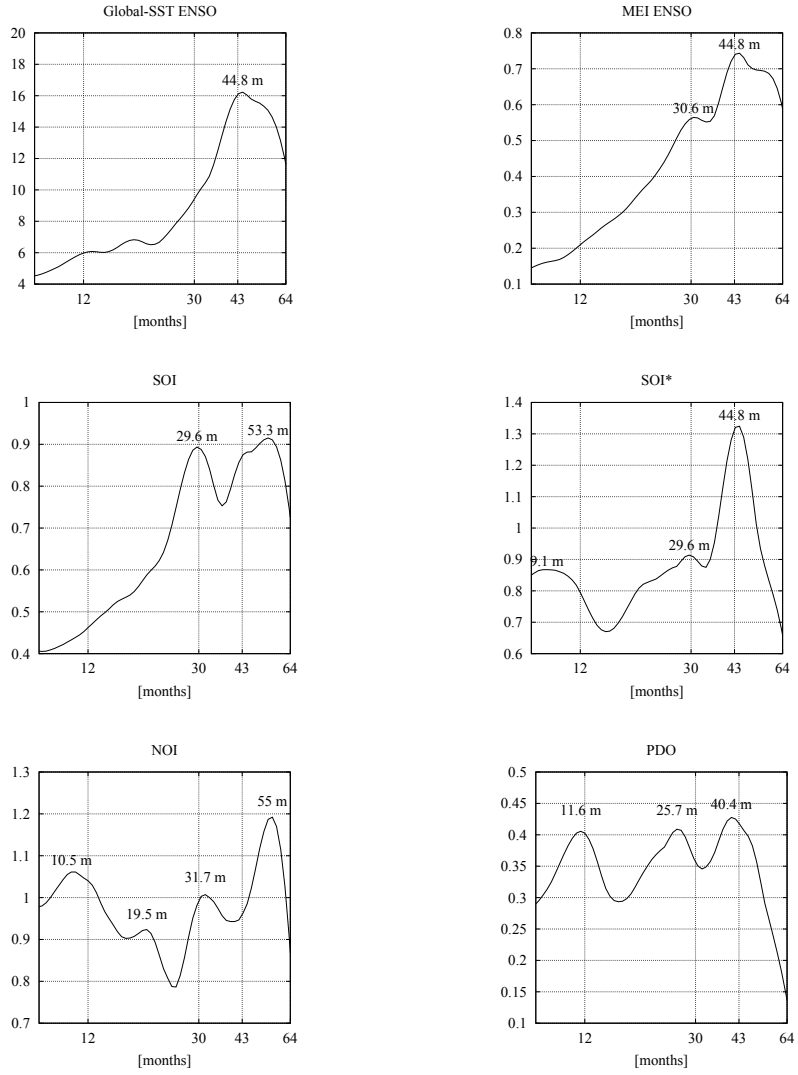

Fig. 14. Scale spectra of the climatic indices related to the Southern Oscillation.

where η_n is a Gaussian white noise with zero mean and unit variance (see e.g. Janacek (2001)).

- The artificial signal (y_n) associated to (x_n) is defined by replacing (δ_n) with (ϵ_n), $y_n = m_n + \epsilon_n$.

Let us remark that (y_n) is indeed a stochastic process; several simulations of the same signal (x_n) will thus yield different realizations.

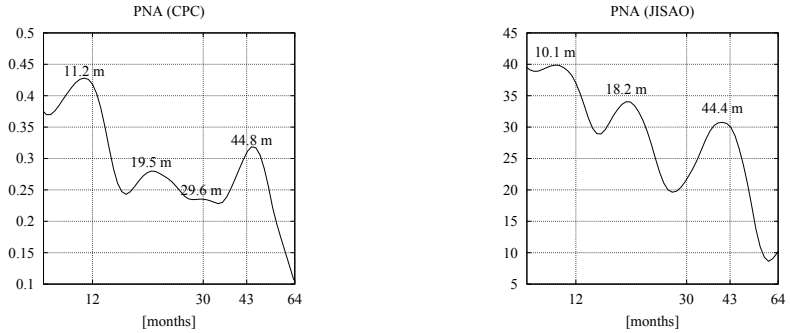

Fig. 15. Scale spectra of the PNA indices.

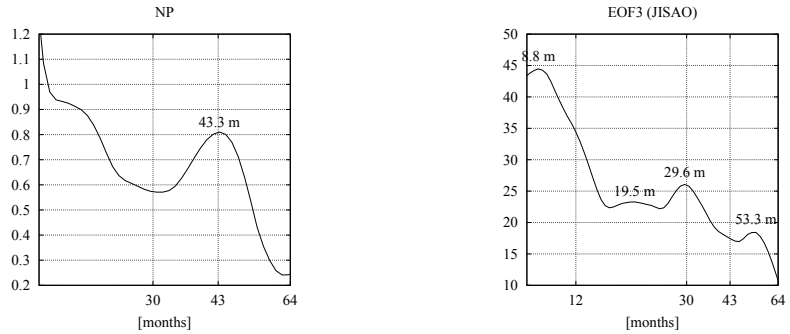

Fig. 16. Scale spectra of other climatic indices.

To check if the cycles c_1 and c_2 appearing in the time series did not occur by pure chance, the subsequent methodology can be applied to each temperature time series (x_n) of the NCEP/NCAR reanalysis data:

- $N = 10,000$ realizations (y_n) of (x_n) are computed.
- The distribution of the highest local maximum y_M of the scale spectrum of the data in the range of 26 to 47 months is estimated from these artificial signals, i.e. one computes the distribution of
$$y_M = \sup_{26 \leq a \leq 47} \tilde{\Lambda}(a),$$
where $\tilde{\Lambda}$ is the scale spectrum of a realization (y_n).
- The probability P to obtain a maximum of higher amplitude than the one corresponding to c_1 or c_2 observed in the scale spectrum of (x_n) is finally computed, using the distribution previously obtained.

It is shown in Nicolay et al. (2010) that such a methodology yields reliable data. The probability values concerning c_1 and c_2 are displayed in Fig. 17 and Fig. 18 respectively. The coloured area correspond to regions where the cycle is significant. These figures show that most of the

cycles associated with c_1 and c_2 can be considered as significant. The cycle observed in the climatic indices are also significant, since one always get $P < 0.1$ (see Mabille & Nicolay (2009); Nicolay et al. (2010)).
Finally, let us remark that c_1 and c_2 can also be detected through the Fourier transform, if the time series are preprocessed in order to free the corresponding spectrum from the dominating cycle corresponding to one year (for more details, see Nicolay et al. (2010)).

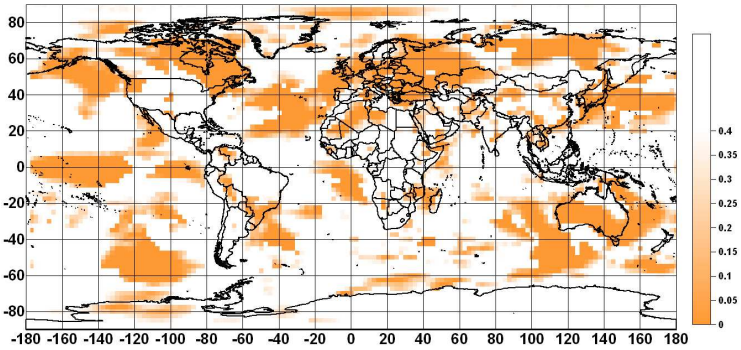

Fig. 17. The probability values associated with c_1 (NCEP/NCAR reanalysis data). The cycles observed in a zone corresponding to the colour white are not significant.

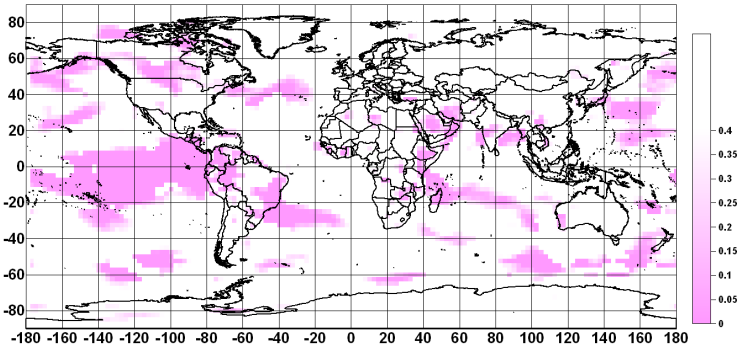

Fig. 18. The probability values associated with c_2 (NCEP/NCAR reanalysis data). The cycles observed in a zone corresponding to the colour white are not significant.

5. Discussion and conclusions

The wavelet-based tool introduced in Sect. 3.1 provides a methodology for detecting cycles in non-stationary signals. Its application to climatic time series has led to the detection of two statistically significant periods of 30 and 43 months respectively.
When looking at the global temperature time series, since most of the lands are situated on the Northern Hemisphere, the cycle c_1 seems to be influenced by the continents, while the cycle c_2 appears to be more influenced by the oceans. However, considering that only a small number

of stations is taken into account in the construction of these records, the above comment has to be taken with circumspection.
Weather station records and NCEP/NCAR reanalysis show that the cycle c_1 is mainly seen in the regions under the influence of the Arctic Oscillation, while the cycle c_2 is observed all over the globe, but more frequently in the regions under the influence of the Southern Oscillation. As a matter of fact, the same cycles are observed in the corresponding indices. In particular c_1 is observed in the spectrum of the AO index and c_2 is detected in the ENSO indices.
As observed in Mabille & Nicolay (2009); Nicolay et al. (2009), the temperature amplitude induced by these cycles always lies between 0.2 and 0.8 K and represents about ten percents of the annual amplitude.
Since the sun is one of the origins of the air mass flows and since the cycles c_1 and c_2 are observed in both the temperature time series and the indices describing the air mass flows, a possible explanation for the existence of these cycles is the solar activity variability. If such hypothesis is true one should find a corresponding cycle in the solar indices such as the solar flux and the sun spot number. Indeed, a cycle corresponding to a period of about 37 months is observed in these data (see Nicolay et al. (2009)). The climate regions could then induce a change of period going from 30 months for continental climates to 43 months for oceanic climates. This cycle corresponding to 37 months detected in the sun is a "flip-flop" type behavior: following Mursula & Hiltula (2004), the solar rotation periodicity undergoes a phase reversal cycle. In Takalo & Mursula (2002), this period is estimated to be about 38 months in the last 40 years, in good agreement with findings based on long series sunspot observations obtained in Berdyugina & Usoskin (2003).

6. References

Allen, M.R. & Robertson, A.W. (1996). *Distinguishing modulated oscillations from coloured noise in multivariate datasets*, Clim. Dyn., 12, 775–784.

Arneodo, A.; Audit, B.; Decoster, N.; Muzy, J.-F. & Vaillant, C. (2002). Climate Disruptions, Market Crashes and Heart Attacks, In: *The Science of Disaster*, A. Bunde and H.J. Sc heelnhuber, (Eds.), pp. 27–102, Springer, Berlin.

Baldwin, M.P. et al. (2001). The quasi-biennial oscillation. *Rev. Geophys.*, Vol. 39, 179–229.

Barnston, A. & Livezey, R. (1987). Classification, seasonality and persistence of low-frequency atmospheric circulation patterns. *Mon. Wea. Rev.*, Vol. 115, 1083–1126.

Berdyugina, S.V. & Usoskin, I.G. (2003). Active longitutes in sunspot activity: Century scale persistence. *Astron. Astrophys.*, Vol. 405, 1121.

Brohan, P.; Kennedy, J.J.; Harris, I.; Tett, S.F.B. & Jones P.D. (2006). Uncertainty estimates in regional and global observed temperature changes: A new dataset from 1850. *J. Geophys. Res.*, Vol. 111, D12,106.

Daubechies, I. (1992). *Ten lectures on wavelets*, SIAM, Philadelphie.

Fedorov, A.V. & Philander, S.G. (2000). Is El Niño changing? *Science*, Vol. 288, 1997–2002.

Freysz, E.; Pouligny, B.; Argoul, F. & Arneodo, A. (1990). Optical wavelet transform of fractal aggregates. *Phys. Rev. Lett.*, Vol. 64, pp. 745–748.

Goupillaud, P.; Grossman, A. & Morlet, J. (1984). Cycle-octave and related transforms in seismic signal analysis. *Geoexploration* , Vol. 23, 85–102.

Hansen J.; Ruedy R.; Glascoe, J. & Sato M. (1999). GISS analysis of surface temperature change. *J. Geophys. Res.*, Vol. 104, 30997–31022.

Huang, N.E. et al. (1998). The empirical mode decomposition and Hilbert spectrum for non-linear and non-stationary time series analysis. *Proc. Roy. Soc. London A*, Vol. 454, pp. 903–995.

Hurrell, J.W. (1995). Decadal trends in the North Atlantic Oscillation: regional temperatures and precipitation. *Science*, 269, 676–679.

Janacek, G. (2001). *Practical time series*, Arnold, London.

Jones, P.D.; Jonsson, T. & Wheeler, D. (1997). Extension to the North Atlantic Oscillation using early instrumental pressure observations from Gibraltar and South-West Iceland. *International Journal of Climatology*, Volume 17, 1433–1550.

Jones, P.D. et al. (2001). Adjusting for sampling density in grid box land and ocean surface temperature time series. *J. Geophys. Res.*, Vol. 106, 3371–3380.

Kalnay, E. et al. (1996). NCEP/NCAR 40-year reanalysis project. *Bull. Amer. Meteor. Soc.*, Vol. 77, 437–471.

Keller, W. (2004). *Wavelets in geodesy and geodynamics*, de Gruyter, Berlin.

Klein Tank, A.M.G. et al. (2002). Daily dataset of 20th-century surface air temperature and precipitation series for the European climate assessment. *International Journal of Climatology*, Vol. 22, 1441–1453.

Klingbjer, P. & Moberg A. (2003). A composite monthly temperature record from Torneladen in Northern Sweden, 1802–2002. *International Journal of Climatology*, Vol. 23, 1465–1494.

Kronland-Martinet, R.; Morlet, J. & Grossmann, A. (1987). Analysis of sound patterns through wavelet transforms. *Int. J. Pattern Recogn. Artific. Intellig.*, Vol. 1, 273–302.

Mabille, G. & Nicolay, S. (2009). Multi-year cycles observed in air temperature data and proxy series. *Eur. Phys. J. Special Topics*, Vol. 174, 135–145.

Mallat, S. (1999). *A wavelet tour of signal processing*, Academic Press, New-York.

Mantua, N.J.; Hare S.R.; Zhang, Y.; Wallace, J.M. &, Francis, R.C. (1997). A pacific interdecadal climate oscillation with impacts on salmon production. *Bulletin of the American Meteorological Society*, Vol. 78, 1069–1079.

Mann, M.E. & Lees, J. (1996). Robust estimation of background noise and signal detection. *Climatic Change*, 33, 409–445.

Mann, M.E.; Rutherford, S.; Wahl, E. & Ammann, C. (2007). Robustness of proxy-based climate field reconstruction methods. *J. Geophys. Res.*, 112, D12109.

Matyasovszky, I. Improving the methodology for spectral analysis of climatic time series. *Theor. Appl. Climatol.*, to appear, DOI: 10.1 007/s00704-009-0212-z.

Meyer, Y. (1989). *Ondelettes et opérateurs*, Hermann, Paris.

Mursula, K. & Hiltula, T. (2004). Systematically asymmetric heliospheric magnetic field: Evidence for a quadrupole mode and non-axis symmetry with polarity flip-flops. *Sol. Phys.*, Vol. 224, 133–143.

Nelder, J. &, Mead R. (1965). A simplex method for function minimization. *Comput. J.*, Vol. 7, 308–313.

Newton, H. & Milsom, A. (1955). Note on the observed differences in spottedness of the Sun's Northern and Southern Hemispheres. *Monthly Not. R. Astron. Soc.*, Vol. 115, 398:404.

Nicolay, S. (2006). *Analyse de séquences ADN par la transformée en ondelettes*, Ph.D. Thesis, University of Liège.

Nicolay, S.; Mabille, G.; Fettweis, X. & Erpicum, M. (2009). 30 and 43 months period cycles found in air temperature time series using the Morlet wavelet method. *Clim. Dyn.*, Vol. 33, pp. 1117–1129.

Nicolay, S.; Mabille, G.; Fettweis, X. & Erpicum, M. (2010). A statistical validation for the cycles found in air temperature data using a Morlet wavelet-based method. *Nonlin. Processes Geophys.*, 17, 269-272.

Paluš, M. & Novotná, D. (2006). Quasi-biennal oscillations extracted from monthly NAO index and temperature records are phase-synchronized. *Nonlin. Processes Geophys.*, Vol. 13, 287–296.

Percival, D.B. & Walden, A.T. (1993). *Spectral analysis for physical applications*, Cambridge University Press, Cambridge.

Rayner, N.A. et al. (2006). Improved analyses of changes and uncertainties in sea surface temperature measured in situ since the mid-nineteenth century: The HadSST2 dataset. *Journal of Climate*, Vol. 19, 446–469.

Rudloff, W. (1981). *World Climates*. Wissenschaftliche Verlagsgesellschaft mbH, Stuttgart.

Ruskai, M.B.; Beylkin, G.; Coifman, R.; Daubechies, I.; Mallat, S.; Meyer, Y. & Raphael, L. (eds.) (1992). *Wavelets and their Applications*, Jones and Bartlett, Boston.

Schwing, F.; Murphree, T. & Green, P. (2002). The northern oscillation index (NOI): A new climate index for the northeast pacific. *Progress in Oceanography*, Vol. 53, 115–139.

Smith, T.M. & Reynolds, R.W. (1997). Extended reconstruction of global sea surface temperature based on COADS data. *J. Climate*, Vol. 16, 1495–1510.

Smith, D.; Cusack, S.; Colman, A.; Folland, C.; Harris, G. & Murphy, J. (2007). Improved surface temperature prediction for the coming decade from global climate model. *Science*, 317, 796–799.

Takalo, J. & Mursula, K. (2002). Annual and solar rotation periodicities in IMF components: Evidence for phase/frequency modulation. *Geophys. Res. Lett.*, Vol. 29, 31–1–31–4.

Titchmarsh, E.C. (1948). *Introduction to the theory of Fourier integrals*, Oxford University Press.

Torresani, B. (1995). *Analyse continue par ondelettes*, CNRS Éditions, Paris.

Trenberth, K. & Hurrell, J.W. (1994). Decadal atmosphere-ocean variations in the pacific. *Climate Dynamics*, Vol. 9, 303–319.

Wolter, K. & Timlin, M.S. (1993). Monitoring ENSO in COADS with a seasonally adjusted principal component index. *Proc of the 17th Climate Diagnostics Workshop*, Norman, OK, NOAA/N MC/CAC, NSSL, Oklahoma Clim. Survey, CIMMS and the School of Meteor, 52–57.

Wolter, K. & Timlin, M.S. (1998). Measuring the strength of ENSO events – how does 1997–98 rank. *Weather*, Vol. 53, 315–324.

Zhang, Y., Wallace, J.M. & Battisti, D.S. (1997). ENSO-like interdecadal variability. *J. Climate*, Vol. 10, 1004–1020.

Zhou, S.; Miller, A.J.; Wang, J. & Angell, J.K. (2001). Trends of NAO and AO and their associations with stratospheric processes. *Geophys. Res. Lett.*, Vol. 28, 4107–4110.